4

Morphological Image Processing Applied in Biomedicine

Roberto A. Lotufo, Leticia Rittner, Romaric Audigier, Rubens C. Machado, and André V. Saúde

Summary. This chapter presents the main concepts of morphological image processing. Mathematical morphology has application in diverse areas of image processing such as filtering, segmentation and pattern recognition, applied both to binary and gray-scale images. Section 4.2 addresses the basic binary morphological operations: erosion, dilation, opening and closing. We also present applications of the primary operators, paying particular attention to morphological reconstruction because of its importance and since it is still not widely known. In Sect. 4.3, the same concepts are extended to gray-scale images. Section 4.4 is devoted to watershed-based segmentation. There are many variants of the watershed transform. We introduce the watershed principles with real-world applications. The key to successful segmentation is the design of the marker to eliminate the over-segmentation problem. Finally, Sect. 4.5 presents the multi-scale watershed to segment brain structures from diffusion tensor imaging, a relatively recent imaging modality that is based on magnetic resonance.

4.1 Introduction

There are several applications of Morphological Processing (MP) in diverse areas of biomedical image processing. Noise reduction, smoothing, and other types of filtering, segmentation, classification, and pattern recognition are applied to both binary and gray-scale images. As one of the advantages of MP, it is well suited for discrete image processing and its operators can be implemented in digital computers with complete fidelity to their mathematical definitions. Another advantage of MP is its inherent building block concept, where any operator can be created by the composition of a few primitive operators.

This text introduces and highlights the most used concepts applied to real situations in biomedical imaging, with explanations based on a morphological intuition of the reader, whenever possible. However, although the lack of full details, the text is as coherent as possible to the mathematical theory and the motivated reader is invited to investigate the many texts, where

T.M. Deserno (ed.), *Biomedical Image Processing*, Biological and Medical Physics, Biomedical Engineering, DOI: 10.1007/978-3-642-15816-2_4,

these details and formalisms are treated in depth [1, 2]. In this chapter, only the main mathematical equations are given. Source codes of implementations of these equations are available on the toolbox IA870 in the Adessowiki[1] project [3]. Other text with example applications from image microscopy using this toolbox is also available [4].

Morphological image processing is based on probing an image with a structuring element and either filtering or quantifying the image according to the manner in which the structuring element fits (or does not fit) within the image. By marking the locations at which the structuring element fits within the image, we derive structural information concerning the image. This information depends on both the size and shape of the structuring element. Although this concept is rather simple, the majority of operations presented in this chapter is based on it: erosion, dilation, opening, closing, morphological reconstruction, etc., applied both for binary and gray-scale images.

In this chapter, only symmetric structuring elements will be used. When the structuring element is asymmetric, care must be taken as some properties are valid for a reflected structuring element. Four structuring elements types will be used in the illustrations and demonstrations throughout this chapter:

- *cross*: the elementary cross is a 3×3 structuring element with the central pixel and its four direct neighbors (4-neighborhood).
- *box*: the elementary box is a 3×3 structuring element with all nine pixels, the central and its eight neighbors (8-neighborhood).
- *disk*: the disk of a given radius is a structuring element with all pixels that are inside the given radius.
- *line*: the linear structuring element can be composed for a given length and orientation.

4.2 Binary Morphology

4.2.1 Erosion and Dilation

The basic fitting operation of mathematical morphology is erosion of an image by a structuring element. The erosion is computed by scanning the image with the structuring element. When the structuring element fits completely inside the image, the scanning position is marked. The erosion consists of all scanning locations where the structuring element fits inside the image. The erosion of set A by set B is denoted by $A \ominus B$ and defined by

$$A \ominus B = \{x : B_x \subset A\}, \tag{4.1}$$

where $\subset$ denotes the subset relation and $B_x = \{b + x : b \in B\}$ the translation of set B by a point x.

[1] `http://www.adessowiki.org`

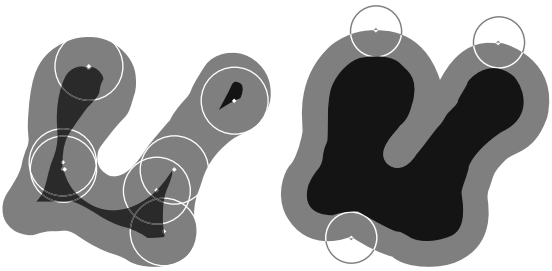

Fig. 4.1. *Erosion and dilation. Left*: input image in black and gray and erosion in black (region where the center of the robot can move); *Right*: input image in black and dilation in black and gray

A binary image is formed by foreground and background pixels. In morphology, for every operator that changes the foreground, there is a dual operator that changes the background. The dual operator for the erosion is the dilation. Since dilation involves a fitting into the complement of an image, it represents a filtering on the outside, whereas erosion represents a filtering on the inside (Fig. 4.1). For intuitive understanding, the structuring element can be seen as a moving robot.

Formally, the dilation of set A by B, denoted by $A \oplus B$, is defined by

$$A \oplus B = (A^c \ominus \breve{B}),^c \tag{4.2}$$

where A^c denotes the set-theoretic complement of A and $\breve{B} = \{-b : b \in B\}$ is the reflection of B, i.e., a 180°-rotation of B about the origin. Foreground is generally associated to white color while background is associated to black color. But note that in impression works, the inverse convention is sometimes used.

Another alternative equivalent way to compute the dilation is by "stamping" the structuring element on the location given by every foreground pixel in the image. Formally, the dilation can also be defined by

$$A \oplus B = \bigcup_{a \in A} B_a. \tag{4.3}$$

Dilation has the expected expanding effect, filling in small intrusions into the image (Fig. 4.1, right) and erosion has a shrinking effect, eliminating small extrusions (Fig. 4.1, left).

As dilation by a disk expands an image and erosion by a disk shrinks an image, both can be used for finding boundaries for binary images. The three possibilities are:

1. *External boundary*: dilation minus the image.
2. *Internal boundary*: the image minus the erosion.
3. *Combined boundary*: dilation minus erosion.

The latter straddles the actual Euclidean boundary and is known as the morphological gradient, which is often used as a practical way of displaying the boundary of the segmented objects.

4.2.2 Opening and Closing

Besides the two primary operations of erosion and dilation, there are two important operations that play key roles in morphological image processing, these being opening and its dual, closing.

The opening of an image A by a structuring element B, denoted by $A \circ B$, is the union of all the structuring elements that fit inside the image (Fig. 4.2, left):

$$A \circ B = \bigcup \{B_x : B_x \subset A\} \quad \text{or} \tag{4.4}$$

$$A \circ B = (A \ominus B) \oplus B. \tag{4.5}$$

It can also be defined as an erosion followed by a dilation (4.5) and has its dual version called closing (Fig. 4.2, right), which is defined by

$$A \bullet B = (A^c \circ \breve{B})^c \quad \text{or} \tag{4.6}$$

$$A \bullet B = (A \oplus B) \ominus B. \tag{4.7}$$

Note that whereas the position of the origin relative to the structuring element has a role in both erosion and dilation, it plays no role in opening and closing. However, opening and closing have two important properties [5]:

1. Once an image has been opened (closed), successive openings (closings) using the same structuring element produce no further effects.
2. An opened image is contained in the original image which, in turn, is contained in the closed image (Fig. 4.2).

As a consequence of this property, we could consider the subtraction of the opening from the input image, called opening top-hat, and the subtraction of the image from its closing, called closing top-hat, respectively, defined by

$$A \hat{\circ} B = A - (A \circ B) \quad \text{and} \tag{4.8}$$

$$A \hat{\bullet} B = (A \bullet B) - A. \tag{4.9}$$

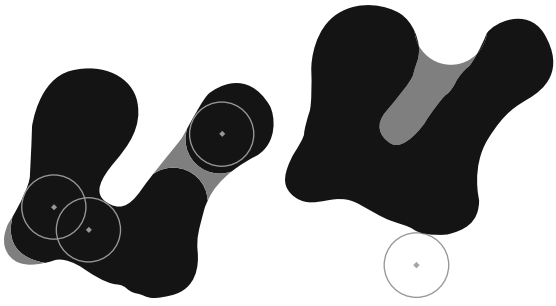

Fig. 4.2. *Opening and closing. Left*: input image in black and gray and opening in black (region where the robot can move); *Right*: input image in black and closing in black and gray

Opening top-hat and closing top-hat correspond to the gray parts of Fig. 4.2 left and right, respectively.

As a filter, opening can clean the boundary of an object by eliminating small extrusions; however, it does this in a much finer manner than erosion, the net effect being that the opened image is a much better replica of the original than the eroded image (compare left parts of Figs. 4.2 and 4.1). Analogous remarks apply to the closing, the difference being the filling of small intrusions (compare right parts of Figs. 4.2 and 4.1).

When there is both union and subtractive noise, one strategy is to open to eliminate union noise in the background and then close to fill subtractive noise in the foreground. The open-close strategy fails when large noise components need to be eliminated but a direct attempt to do so will destroy too much of the original image. In this case, one strategy is to employ an Alternating Sequential Filter (ASF). Open-close (or close-open) filters are performed iteratively, beginning with a very small structuring element and then proceeding with ever-increasing structuring elements.

The close-open filter is given by

$$ASF^{n}_{oc,B}(S) = (((((S \bullet B) \circ B) \bullet 2B) \circ 2B) \ldots \bullet nB) \circ nB \tag{4.10}$$

and the open-close filter by

$$ASF^{n}_{co,B}(S) = (((((S \circ B) \bullet B) \circ 2B) \bullet 2B) \ldots \circ nB) \bullet nB, \tag{4.11}$$

where $nB = B + B + ... + B$ (n times).

4.2.3 Morphological Reconstruction from Markers

One of the most important operations in morphological image processing is reconstruction from markers, the basic idea being to mark some image components and then reconstruct that portion of the image consisting of the marked components.

Given a neighborhood relationship, a region (collection of pixels) is said to be connected if any two pixels in the region can be linked by a sequence of neighbor pixels also in the region. 4-neighborhood and 8-neighborhood are usual neighborhoods that include vertically and horizontally adjacent pixels and, only for the latter one, diagonally adjacent pixels.

Every binary image A can be expressed as the union of connected regions. If each of these regions is maximally connected, which means that it is not a proper subset of a larger connected region within the image, then the regions are called connected components of the image. The union of all connected components C_k recovers the input image A and the intersection of any two connected components is empty.

To find all the connected components of an image, one can iteratively find any pixel of the image, use it to reconstruct its connected component, remove the component from the image, and iteratively repeat the same extraction

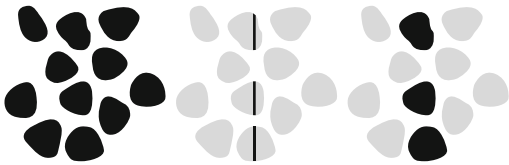

Fig. 4.3. *Reconstruction from markers. Left*: input image, *Middle*: marker image; *Right*: reconstructed image

until no more pixels are found in the image. This operation is called labeling (cf. panel (c) in Fig. 4.5). The labeling decomposes an image into its connected components. The result of the labeling is usually stored in a numeric image with each pixel value associated to its connected component number.

The morphological reconstruction of an image A from a marker M (a subset of A) is denoted by $A \triangle M$ and defined as the union of all connected components of image A that intersect marker M. This filter is also called component filter:

$$A \triangle M = \bigcup \{C_k : C_k \cap M \neq \emptyset\}. \tag{4.12}$$

In addition to the input image and the marker, the reconstruction operation also requires a connectivity. The marker informs which component of the input image will be extracted, and the connectivity can be specified, in some software packages, by a structuring element, usually the elementary cross for 4-neighborhood or the elementary box to specify 8-neighborhood.

An example of reconstruction from markers, based on 8-connectivity, is shown in Fig. 4.3. The input image is a collection of grains. The markers are made of a central vertical line intersecting the grains. The reconstruction from the markers extracts the three central components from the original image.

There are typically three ways to design the marker placement for the component filter:

1. A-priori selection,
2. Selection from the opening, or
3. Selection by means of some rather complex operation.

The edge-off operation, particularly useful to remove objects touching the image frame, combines reconstruction and top-hat concepts. The objects touching the frame are selected by reconstructing the image from its frame as an a priori marker. The objects not connected to the image frame are selected by subtracting the input image from the reconstructed image.

4.2.4 Reconstruction from Opening

With marker selection by opening, the marker is found by opening the input image by a structuring element. The result of the reconstruction detects all connected components where the structuring element fits.

Using the same mechanism of the reconstruction from opening to detect objects with particular geometric features, more complex techniques can be

designed to find the markers from combined operators. At the last step, the reconstruction reveals the objects that exhibit those features.

The following biomedical application (Fig. 4.4) detects overlapping chromosomes. To identify overlapping chromosomes (Fig. 4.4, panel (b)) only the shapes (connected components) are chosen that all the four linear structuring elements can fit. This is achieved by intersecting the four reconstructions from opening using four linear structuring elements: vertical, horizontal, 45°, and −45°, as visualized in Fig. 4.4 on panels (c), (d), (e), and (f), respectively.

The top-hat concept can be applied to reconstruction by opening producing the reconstruction from opening top-hat (i.e., the image minus its reconstruction). In this case, the operator reveals the objects that do not exhibit a fitting criterion. For instance, to detect thin objects, one can use a disk of diameter larger than the thickest of the thin objects.

Another common criterion for selection of connected component is its area. This is achieved by the area opening which removes all connected component C_i with area less than a specified value α:

$$A \circ (\alpha)_E = \bigcup \{C_i,\ \text{area}(C_i) \geq \alpha\}. \tag{4.13}$$

The next demonstration targets cytogenetic images of meta-phase human cells. This is a classification application of area opening. The task is to preprocess the image by segmenting the chromosomes from the nuclei, stain debris and the background. Figure 4.5 shows the input image (a), the thresholded (b), the labeling (c) identifying the connected components, and the result (d) with the components classified by area. The components with area less than

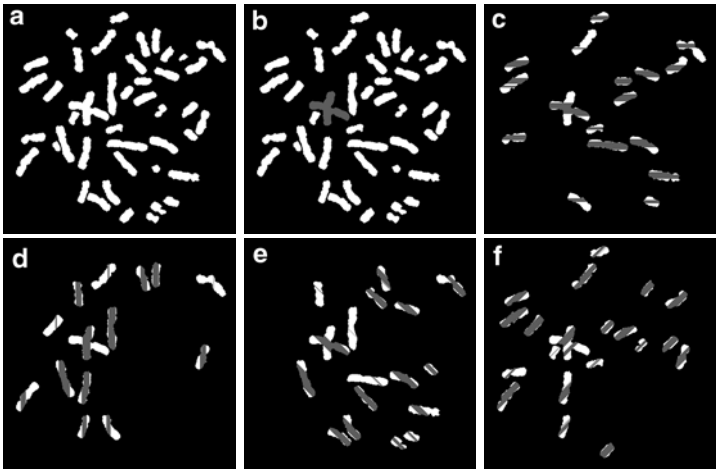

Fig. 4.4. *Detecting overlapping chromosomes.* (**a**) Input image; (**b**) intersection (*in gray*) of four reconstruction from openings; (**c**) opening (*in gray*) by horizontal line and its reconstruction; (**d**) opening (*in gray*) by vertical line and its reconstruction; (**e**) opening (*in gray*) by 45°-line and its reconstruction; and (**f**) opening (*in gray*) by −45°-line and its reconstruction

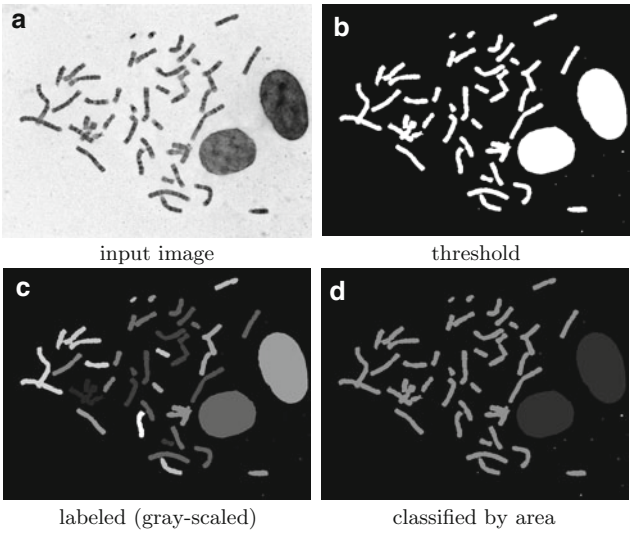

Fig. 4.5. *Chromosome spreads and area opening.* Residues are coded in white (area less than 100), chromosomes in light gray (area between 100 and 10,000), and nuclei in dark gray (area larger than 10,000)

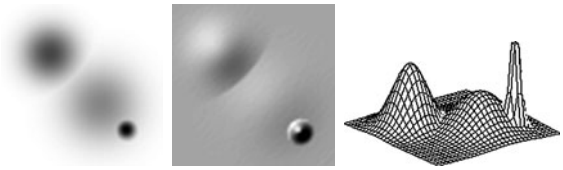

Fig. 4.6. *Representation of a gray-scale image. Left*: gray-scale mapping, zero is bright and 255 is dark; *Middle*: top-view shading surface; *Right*: surface mesh plot

100 pixels are background noise, the ones with area larger than 10,000 pixels are nuclei (dark gray) and the rest are the chromosomes (light gray).

So as not to be restricted to openings, analogous dual concepts can be developed to form sup-reconstruction from closing, sup-reconstruction from closing top-hat and area closing.

4.3 Gray-Scale Operations

It is useful to look at a gray-scale image as a surface. Figure 4.6 shows a gray-scale image made of three Gaussian-shape peaks of different heights and variances. The image is depicted in three different graphical representations: (a) the inverted print, where the pixel values are mapped in a gray scale: low values are bright and high values are dark gray tones; (b) a top-view shading surface; and (c) a mesh plot of the surface.

A gray-scale image can also be seen as the cardboard landscape model, i.e., a stack of flat pieces of cardboard. Thus, the threshold decomposition of a gray-scale image f is the collection of all the threshold sets $X_t(f)$ obtained at each gray level t:

$$X_t(f) = \{z : f(z) \geq t\}. \tag{4.14}$$

The image can be characterized uniquely by its threshold decomposition collection and can be recovered from its threshold sets by stack reconstruction:

$$f(x) = \max\{t : x \in X_t(f)\}. \tag{4.15}$$

In all gray-scale operations presented hereafter, we will use flat structuring elements, i.e., structuring elements that have no gray-scale variation, the same used in the binary case. Although they are the same structuring elements, we will use the term flat structuring elements not to confuse with their gray-scale versions. This restriction has many simplifications in the definition, characterization and use of the gray-scale operators as an extension from the binary operators. Care must be taken however, when the reader uses a gray-scale structuring element, as the erosion (dilation) is not a moving minimum (moving maximum) filter, the threshold decomposition property does not hold for the primitive operators nor for gray-scale morphological reconstruction. Moreover, as we said before, only symmetric structuring element will be used.

4.3.1 Erosion and Dilation

Gray-scale erosion (dilation) of an image f by a flat structuring element D is equivalent to a moving minimum (moving maximum) filter over the window defined by the structuring element. Thus, erosion $f \ominus D$ and dilation $f \oplus D$ in this case are simply special cases of order-statistic filters:

$$(f \ominus D)(x) = \min\{f(z) : z \in D_x\} \text{ and} \tag{4.16}$$

$$(f \oplus D)(x) = \max\{f(z) : z \in D_x\}. \tag{4.17}$$

An example of gray-scale erosion by a disk on a gray-scale image is shown in Fig. 4.7. The two images on the left, input and eroded, are represented in gray-scale shades and the two on the right are the same images represented by their top-view surfaces. Note how well the term "erosion" applies to this illustration. The eroded surface appears as being created by a pantograph engraving machine equipped with a flat disk milling cutter. The pantograph is guided to follow the original surface while shaping the eroded surface using the flat disk milling cutter.

The geometric intuition for erosion is the following: slide the structuring element along beneath the surface and at each point record the highest altitude the location of the structuring element can be translated while fitting beneath the surface.

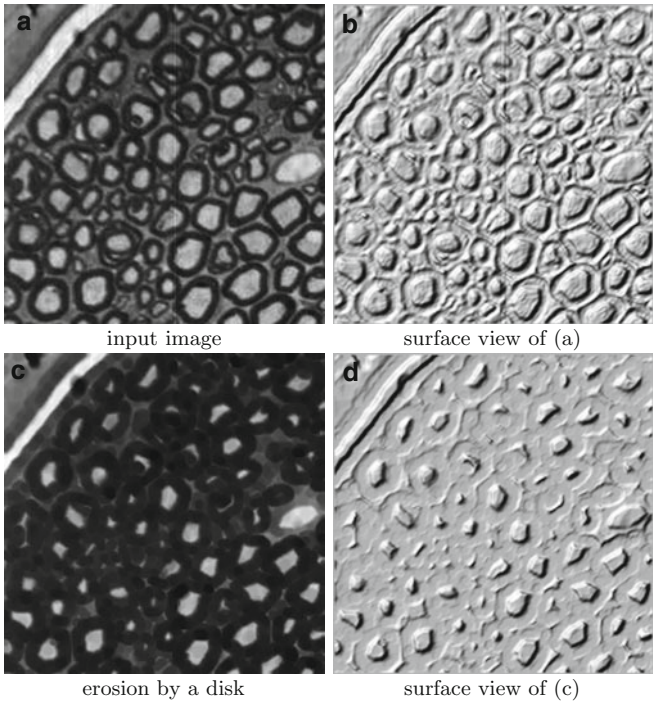

Fig. 4.7. *Gray-scale erosion*

Alternatively, one can simply compute the erosion (dilation) of a gray-scale image by computing the stack decomposition of the image, applying binary erosion (dilation) on the threshold sets, and finally stack reconstruction.

Figure 4.8 illustrates the discrete gray-scale erosion by means of threshold decomposition. At the right of the gray-scale images (original and eroded), there are three threshold sets at gray levels 80, 120, and 180. Note that the binary images shown in (f), (g), and (h) are eroded versions of the binary images shown in (b), (c), and (d).

Observe that the morphological gradient, described for binary pictures, is directly extensible to gray-scale with gray-scale erosions and dilations (dilation minus erosion). At each point, the morphological gradient yields the difference between the maximum and minimum values over the neighborhood at the point determined by the flat structuring element.

4.3.2 Opening and Closing

As an extension of the binary case, gray-scale opening (closing) can be simply achieved by stack decomposition, binary opening (closing), and stack reconstruction.

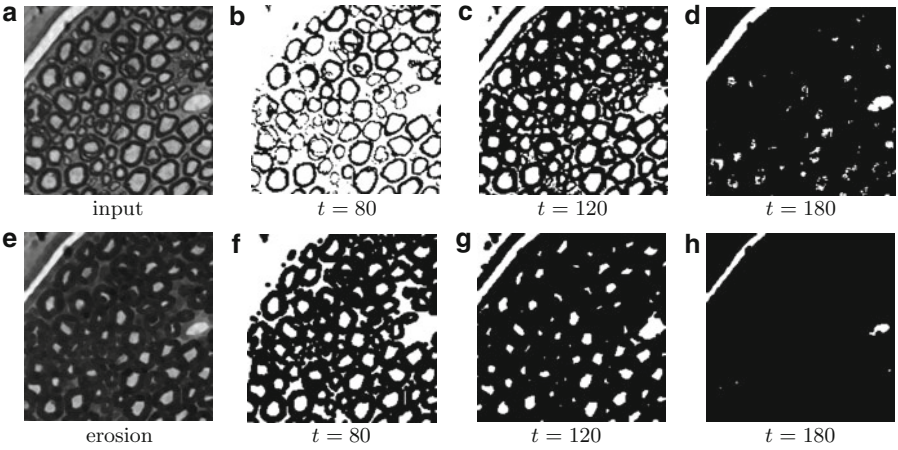

Fig. 4.8. *Gray-scale erosion by threshold decomposition.* The threshold sets are indicated by the threshold t

The geometric intuition for opening is the following: slide the structuring element along beneath the surface and at each point record the highest altitude the structuring element can be translated while fitting beneath the surface. The position of the origin relative to the structuring element is irrelevant. Note the slight difference between the opening and the erosion: while in the opening the highest altitude is recorded for all points of the structuring element, in the erosion, only the location of the structuring element is recorded.

Geometric intuition regarding closing can be obtained from the duality relation. Whereas opening filters from below the surface, closing filters from above; indeed, by duality, closing is an opening of the negated image.

The gray-scale opening and closing have the same properties of their binary equivalents [6]. The top-hat concept is also valid: gray-scale opening top-hat is given by the subtraction of the opened image from the input image, and the gray-scale closing top-hat is the subtraction of the image from its closing.

Open top-hat is very useful as a preprocessing step to correct uneven illumination before applying a threshold, thereby acting as an adaptive thresholding technique. The following application illustrates this.

Figure 4.9 shows the open top-hat transform applied to a Fluorescent In-Situ Hybridization (FISH) image. FISH is a key technique for molecular diagnosis in which labeled hybridizing agents (such as Deoxyribonucleic Acid (DNA) or Ribonucleic Acid (RNA) probes) are exposed to intact tissue sections. The probe hybridizes to a defined target nucleotide sequence of DNA in the cell. Each chromosome containing the target DNA sequence will produce a fluorescent signal (spot) in every cell when the specimen is illuminated with suitable excitation. Hence, FISH is an excellent method for detection of

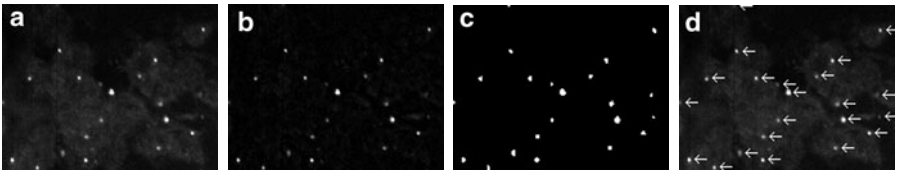

Fig. 4.9. *Gray-scale open top-hat.* (**a**) Input image; (**b**) opening top-hat by a disk of radius 4; (**c**) thresholded area open (by 2 pixels); and (**d**) dilation of centroids by arrow, for illustration, overlaid on original

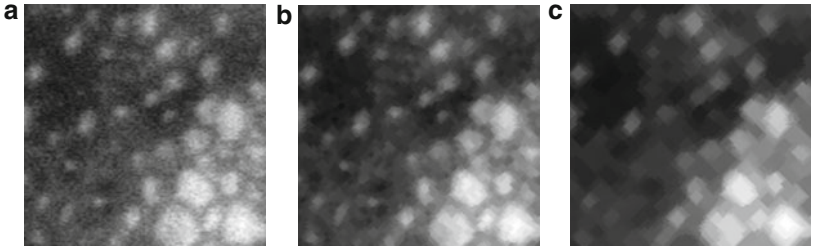

Fig. 4.10. *Gray-scale alternating sequential filtering (ASF)*

gene copy number alterations in cancer and other diseases, and the task of image processing is automatic detection of these spots. Owing to noise, the top-hat methodology typically yields very small spots in the thresholded top-hat image. These can be eliminated by area open. So, the image is filtered by a gray-scale area opening of two. In Fig. 4.9d, the arrows were overlaid automatically by a dilation of the centroids of the detected spots by an arrow-shape structuring element, with the origin slightly translated from the arrow tip so as not to disturb the visualization of the original spots.

Gray-scale opening can be employed to filter noise spikes lying above the signal and the closing can be used to filter noise spikes beneath the image. Typically noise is mixed, there being noise spikes both above and below the signal. So long as these noise spikes are sufficiently separated, they can be suppressed by application of either a composition of opening and closing or of closing and opening. Selection of an appropriately sized structuring element is crucial. In addition, if there is a mixture of unevenly spatially sized noise spikes and they are not sufficiently dispersed, one can employ an ASF, which is a composition of alternating openings and closings with increasingly wide structuring elements (Fig. 4.10). A single stage close-open filter results from closing followed by opening using a 3×3 diamond structuring element. For the second stage, another close-open is concatenated using a 5×5 diamond structuring element. In Fig. 4.10c, a three stage ASF was applied with the last stage being processed by a 7×7 diamond structuring element.

4.3.3 Component Filters and Morphological Reconstruction

The concept of connected component filter built from morphological reconstruction from markers, reconstruction from openings and area open introduced in the binary morphology section can be extended for gray-scale. These binary operators can be used to construct a correspondent gray-scale operator by using the notion of threshold decomposition. The level component in a gray-scale image is defined as a connected set of the pixels in a threshold set of the image at a given level. When modeling the gray-scale image by a cardboard landscape, the cardboard is first cut into the shape of each iso line (i.e., lines of same height), then all pieces are stacked up to form the topography. Each cardboard piece is a connected component of a level set of the gray-scale image. A gray-scale component filter is an operator that selects only a few level components (cardboard pieces) in such a way that the stack reconstruction is not disturbed, i.e., a level component is removed only if all the level components above it are also removed.

Since the notion of connected components is intrinsically related to this section, it is wise to recall that the definition of all component filters require the specification of a connectivity, which is normally the 4- or 8-neighborhood. One important property of a component filter is that it never introduces a false edge, so it is part of the so-called family of edge-preserving smoothing filters.

Morphological reconstruction is one of the most used tools to build component filters [7–9]. As with binary reconstruction, gray-scale reconstruction proceeds from markers. The morphological reconstruction of an image from a marker can be obtained by stack decomposition of the image and the marker, binary reconstructions at each gray-level, and stack reconstruction of the results. This can be intuitively explained by using the cardboard landscape model of the image. Imagine that the cardboard pieces are stacked but not glued. The markers are seen as needles that pierce the model from bottom to top. If one shakes the model while holding the needles, every cardboard pieces not pierced by the needles will be removed. The remaining cardboards constitute a new model that corresponds to the gray-scale morphological reconstruction, also called Inf-reconstruction. By duality, the sup-reconstruction works in the same manner but on the negated image. Observe that the marker can be a gray-scale image, the pixel intensity corresponding to the height the needles reach when they pierce the model.

Gray-scale area opening is another component filter [10]. It is defined analogously to the binary case. The size α area opening of a gray-scale image can be modeled as a stack filter in which at each level, only binary connected components containing at least α pixels are passed: it removes all cardboard pieces whose area is less than α.

An important class of component filters is composed of those generated from alternating reconstructions from openings and closings. They are called Alternating Sequential Component Filter (ASCF).

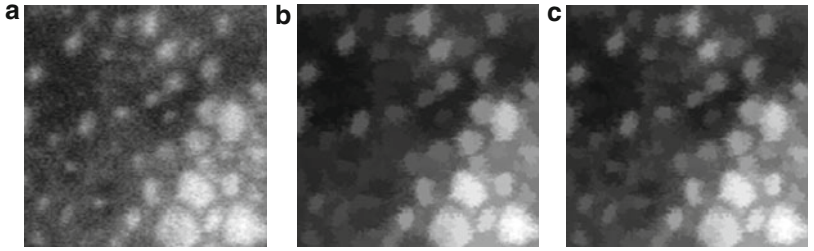

Fig. 4.11. *Gray-scale alternating sequential component filtering (ASCF).* The reconstructive and area close-open was performed with a 3×3 diamond of stage 3 and an area parameter of 30 pixels, respectively

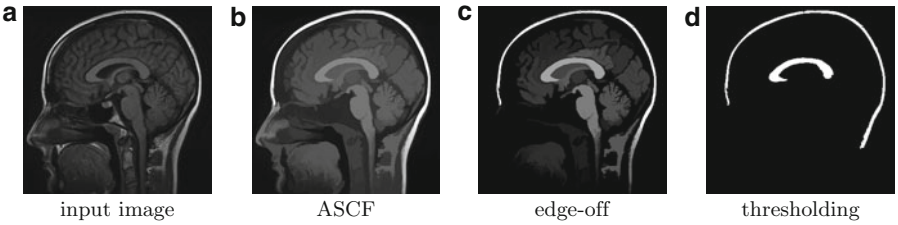

Fig. 4.12. *Segmenting the corpus callosum with gray-scale component filters.* In panel (**b**), an area close-open ASCF is applied

Figure 4.11 shows two examples of gray-scale ASCF using the same input image as in Fig. 4.10. A three stage close-open filter is performed by sup-reconstruction from closing followed by a reconstruction from opening using a 3×3, 5×5, and 7×7 diamond structuring element in the first, second and last stage, respectively. An ASCF area close-open with area parameter of 30 pixels yields similar effects (Fig. 4.10c). Note the high fidelity of the edges maintained by component filters.

The gray-scale edge-off operator can be easily derived from the binary case and it is very useful in many situations. As in the binary case, the edge-off is the top-hat of the reconstruction from a marker placed at the image frame (case where the marker is placed a priori). In the cardboard landscape model (threshold decomposition), all the cardboard pieces that touch the image frame are removed, leaving only the cardboard pieces that form domes inside the image.

The following application illustrates the use of area close-open ASCF as a preprocessing filter followed by the edge-off operator to segment the corpus callosum from an Magnetic Resonance Imaging (MRI) of the brain (Fig. 4.12). The area close-open ASCF is used with area parameter 1,500 pixels, first filling cardboard holes of less than this size, and removing cardboards with area less than 1,500 pixels afterwards. After applying the edge-off operator, a hard segmentation can be obtained by thresholding at level 40.

The reconstruction of an image f from itself subtracted by h is called h-maxima: $\mathrm{HMAX}_{h,D}(f)$. It is a component filter that removes any dome with height less than or equal h and decreases the height of the other domes by h. For a geometric interpretation of the h-maxima based on the threshold decomposition concept, the height attribute associated to a level component (cardboard piece) is one plus the maximum number of levels that exist above it. The h-maxima filter removes all the cardboard pieces with height attribute below or equal to h.

The dual operator of h-maxima is called h-minima: $\mathrm{HMIN}_{h,D}(f)$ fills in any basin of image f with depth less than h and decreases the depth of the other basins by h.

4.3.4 Regional Maxima

Considering the threshold decomposition of a gray-scale image, regional maxima are level components with height attribute equal to one, i.e., there is no other level component above them. These are the cardboard pieces that are on top of a dome. For instance in Fig. 4.18, panel (c) shows the regional maxima of the image in panel (b). All regional maxima of an image f can be found by subtracting the h-maxima with $h = 1$ from image f:

$$\mathrm{RMAX}_D(f) = f - \mathrm{HMAX}_{1,D}(f). \tag{4.18}$$

By duality, a regional minimum is a flat connected region that is at the bottom of a basin. Regional maxima and minima are generically called extrema of the image. Due to the inherent noise associated with the acquisition process, a biomedical image typically presents a large number of regional maxima. If the regional maximum operator is applied to a gradient image, then the situation is even worse. Dynamics provide a tool for selecting significant extrema with respect to a contrast criterion [11]. The dynamics of a regional maximum is the height we have to climb down from the maximum to reach another maximum of higher altitude. The dynamics of a minimum is the minimum height a point in the regional minimum has to climb to reach a lower regional minimum. Filtering the domes of the image also removes regional maxima. Dome filtering can be accomplished using opening, reconstruction from opening, area open, or h-maxima. The choice of appropriate filter is part of the design strategy.

Figure 4.13 shows the regional maxima of the input image following different filters. Note how the over-segmentation given by the direct regional maxima was reduced. These markers can be used to segment the image using the watershed transform. One of the crucial steps in the watershed transform is marker extraction. A marker must be placed in a representative sample of the region of the object to be extracted. The marker finding using the regional maxima (minima) of filtered images is a powerful method since it is independent of gray-scale thresholding values.

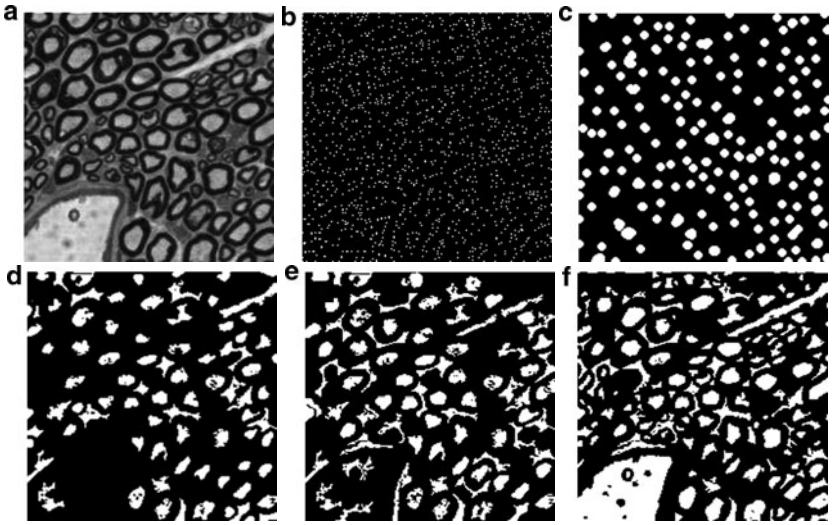

Fig. 4.13. *Regional maxima of filtered image.* (**a**) input image; (**b**)–(**f**) regional maxima; (**c**) after opening by a disk of radius 3; (**d**) after reconstruction from opening by the same disk; (**e**) after area open of 100 pixels; and (**f**) after h-maxima filtering with $h = 40$

4.4 Watershed Segmentation

The watershed transform is a key building block for morphological segmentation [12]. In particular, a gray-scale segmentation methodology results from applying the watershed to the morphological gradient of an image to be segmented. The watershed methodology has become highly developed to deal with numerous real-world contingencies, and a number of implementation algorithms have been developed [13,14]. There are many watershed algorithms in the literature. Here, we only cover the basic methodology.

4.4.1 Classical Watershed Transform

The most intuitive formulation of the watershed transform is based on a flooding simulation. Consider the input gray-scale image as a topographic surface. The problem is to produce the watershed lines on this surface. To do so, holes are punched in each regional minimum of the image. The topography is slowly flooded from below by letting water rise from each regional minimum at a uniform rate across the entire image. When the rising water coming from distinct minima is about to merge, a dam is built to prevent the merging. The flooding will eventually reach a stage when only the tops of dams are visible above the water surface, and these correspond to the watershed lines. The final regions arising from the various regional minima are called the catchment basins.

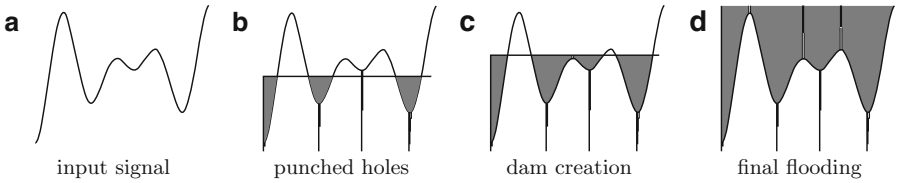

Fig. 4.14. *Flooding simulation of the watershed transform*

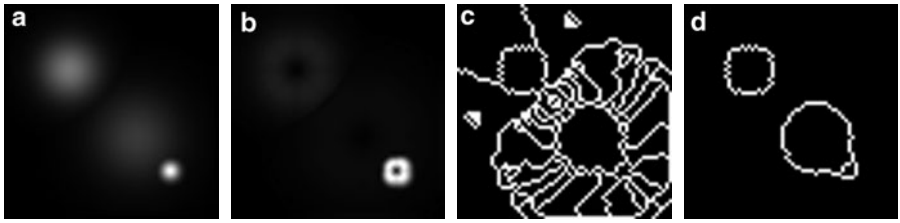

Fig. 4.15. *Classical watershed, regional minima filtering.* (**a**) small synthetic input image (64×64); (**b**) morphological gradient; (**c**) watershed on the morphological gradient; (**d**) watershed on the h-minima ($h = 9$) filtered morphological gradient

Figure 4.14 illustrates this flooding process on a signal with four regional minima generating four catchment basins. At first, holes are punched at the minima (cf. panel (b)). Then, the flooding process is initialized. A dam is created whenever water from different minima are about to merge (cf. panel (c)). The final flooding yielding three watershed lines and four catchment basins (cf. panel (d)).

For image segmentation, the watershed is usually (but not always) applied on a gradient image. As real digitized images present many regional minima in their gradients, this typically results in a large number of catchment basins, the result being called watershed over-segmentation.

4.4.2 Filtering the Minima

A solution to cope with the over-segmentation problem is to filter the image, in order to reduce the number of regional minima, creating less catchment basins. Figure 4.15 shows the typical application of the classical watershed transform. Although the image is synthetic, due to the discretization process there are several regional minima in the image, each one generating one catchment basins. By filtering the gradient image using the h-minima with parameter $h = 9$, the watershed gives the desired result. This kind of filtering is very subtle for our eyes as we cannot distinguish the difference from the original morphological gradient and the filtered one, despite the difference between their number of regional minima.

In Fig. 4.16, watershed over-segmentation is reduced by filtering the minima of the input image with a close by a disk of radius 3 (cf. panel (c));

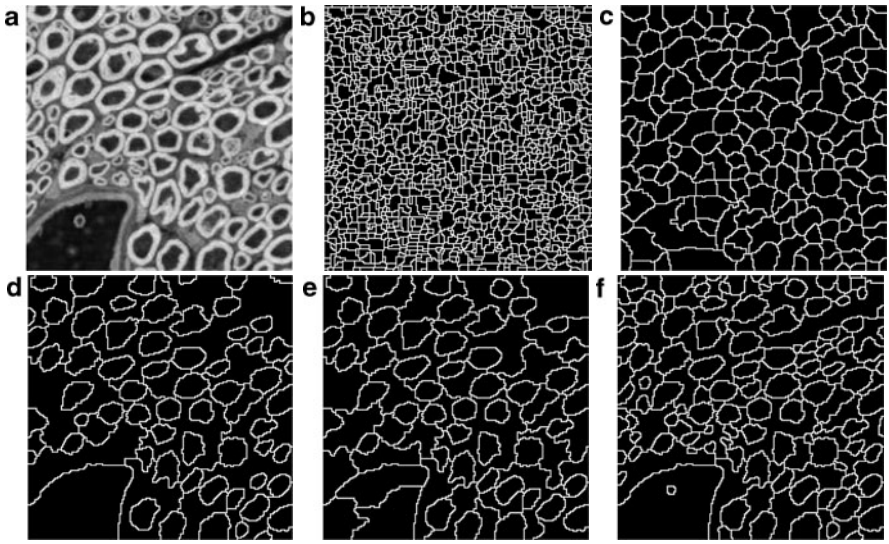

Fig. 4.16. *Reducing over-segmentation by minima filtering.* (**a**) Input image; (**b**) watershed of the input image; (**c**) watershed of the input image after closing by a disk of radius 3; (**d**) watershed of the input image after sup-reconstruction from closing by the same disk; (**e**) watershed of the input image after area open of 100 pixels; and (**f**) watershed of the input image after h-minima filtering with $h = 40$

with sup-reconstruction from closing by the same disk (cf. panel (c)); with area closing (cf. panel (d)); and with h-minimum (cf. panel (f)). This example is equivalent to the regional maxima simplification shown in Fig. 4.13. If we compute the regional minima of the filtered images, we get the same results of that figure. Note that to filter regional minima, the filters used are those that operate with the valleys such as closings and h-minima. Applying filters that operate on domes do not result in any simplification on the number of minima or on the number of catchment basins of the watershed.

4.4.3 Watershed from Markers

Markers are very effective to reduce over-segmentation if one knows how to place the markers within the objects to be segmented. The watershed from markers can also be described as a flooding simulation process (Fig. 4.17). At first, holes are punched at the marker regions and each marker is associated with a color. The topography is then flooded from below by letting colored water rise from the hole associated with its color, this being done for all holes at a uniform rate across the entire image. If the water reaches a catchment basin with no marker in it, then the water floods the catchment basin without restriction. However, if the rising waters of distinct colors are about to

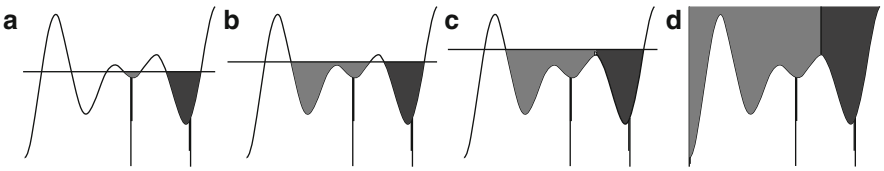

Fig. 4.17. *Flooding simulation of the watershed from markers.* (**a**) punched holes at markers and initial flooding; (**b**) flooding a primitive catchment basin without marker; (**c**) a dam is created when waters coming from different markers are about to merge; (**d**) final flooding, only one watershed line

merge, then a dam is built to prevent the merging. The colored regions are the catchment basins associated with the various markers. To differentiate these catchment basins from the ones obtained with the classical watershed transform, we call the latter primitive catchment basins.

The classical watershed transform can be constructed using the watershed from markers and vice-versa. If we place the markers for the watershed from markers at the regional minima of the input image, then we get the classical watershed transform. To get the watershed from markers from the standard watershed transform is a bit more complicated: we need to apply the classical watershed transform on the sup-reconstruction of the image from the markers.

4.4.4 Inner and Outer Markers

A typical watershed-based segmentation problem is to segment cell-like objects from a gray-scale image. The general approach is threefold:

1. Preprocessing using a smoothing connected filter.
2. Extracting object (inner marker) and background markers (outer marker).
3. Obtaining watershed lines of the morphological gradient from the markers.

Usually, the most crucial part is the extraction of object markers (Step 2): if an object is not marked properly, then it will be missed in the final segmentation.

To illustrate watershed segmentation using inner and outer markers, we consider a poor quality microscopic image of a cornea tissue (Fig. 4.18). The cell markers are extracted by the regional maxima of the opening by a disk of the input image. The criterion used with regional maxima is mainly topological. We can model each cell as a small hill and we want to mark the top of each hill that has a base larger than the disk used in the opening. The regional maxima constitute the inner markers, and the outer markers are obtained by a watershed on the negated input image. After labeling the markers, the morphological gradient is computed. Although it is a very noisy gradient, the final watershed lines provide a satisfactory segmentation.

While it is often the case that the watershed transform is applied to a gradient image, a top-hat image or a distance function image, in some other cases, the input image itself is suitable for application of the watershed.

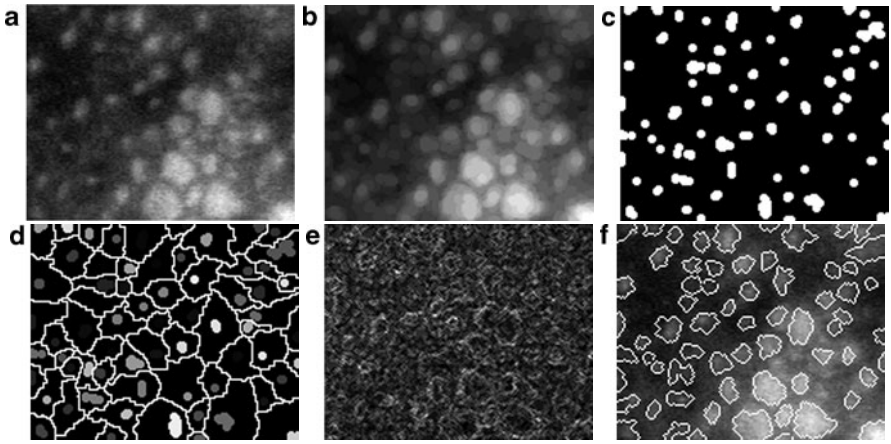

Fig. 4.18. *Segmentation of cornea cells.* (**a**) input image; (**b**) filtered by open; (**c**) regional maxima of the open (inner markers); (**d**) inner and outer markers (watershed lines of the negated input image from the inner markers); (**e**) morphological gradient of the original image; (**f**) final watershed lines overlaid on input image

4.5 Segmentation of Diffusion MRI

Diffusion Tensor Imaging (DTI) is a MRI-based modality able to characterize water molecules diffusion inside tissues and useful to demonstrate subtle brain abnormalities caused by diseases, such as stroke, multiple sclerosis, dyslexia, and schizophrenia [15,16]. However, while most traditional imaging methods in medicine produce gray scale images, DTI produces a tensor valued image (i.e., each pixel or voxel contains a tensor), demanding new, and usually complex, visualization and/or processing methods, cf. Chap. 16, page 403.

One example of DTI can be seen in Fig. 4.19. Each voxel contains a tensor, represented by an ellipsoid, where the main hemiaxis lengths are proportional to the square roots of the tensor eigenvalues λ_1, λ_2, and λ_3 ($\lambda_1 \geq \lambda_2 \geq \lambda_3$) and their directions correspond to the respective eigenvectors.

Several approaches for DTI-based segmentation, where regions of similar diffusion characteristics must be delineated, have been proposed in the last decade [17–22]. One possible solution is to segment DTI using concepts from mathematical morphology, such as the morphological gradient and the watershed transform. Instead of adapting the watershed to work with tensorial images, a tensorial morphological gradient is defined, which translates relevant information from tensors to a scalar map. The desired segmentation is achieved by applying the watershed over this scalar map.

Let $E = \mathbb{Z} \times \mathbb{Z}$ be the set of all points in the tensorial image f. The Tensorial Morphological Gradient (TMG) is defined by

$$\nabla_B^T(f)(x) = \bigvee_{y,z \in B_x} d_n(\boldsymbol{T}_y, \boldsymbol{T}_z), \tag{4.19}$$

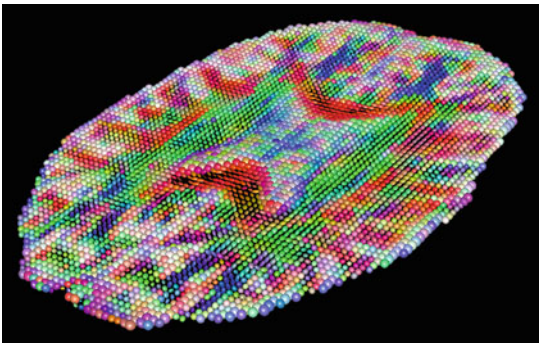

Fig. 4.19. *DTI.* One slice of a diffusion tensor image of the brain. The color of each ellipsoid is related to the principal eigenvector direction of the tensor associated to that voxel

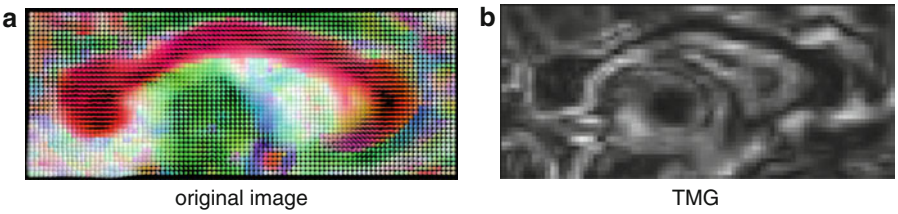

Fig. 4.20. *Tensorial morphological gradient (TMG)*

$\forall x \in E$, where $\bigvee$ is the supremum of a subset, $B \subset E$ is a structuring element centered at the origin of E, d_n represents any of the similarity measures presented in DTI literature [23,24], $\boldsymbol{T}_y$ is the tensor that represents the diffusion in y, and $\boldsymbol{T}_z$ is the tensor that represents the diffusion in z (y and z are in the neighborhood of x, defined by E). ∇_B^T denotes the TMG.

The TMG, as the morphological gradient presented in Sect. 4.2.1, can be used to display the boundary of objects (Fig. 4.20).

Once the tensorial information from DTI is mapped to a gray-scale image, all morphological operators described in Sect. 4.3 can be used to process it. Since the classical watershed transform would lead, in this case, to an over-segmentation, the best choice is to use the hierarchical watershed or Multi-Scale Watershed (MSW) transform, which creates a set of nested partitions. The MSW presented here can be obtained by applying the watershed from markers to a decreasing set of markers. The watershed at scale 1 (finest partitioning) is the classical watershed, made of the primitive catchment basins (perhaps an over-segmentation). As the scale increases, less markers are involved and the coarsest partition is the entire image obtained from a single marker at the regional minimum of largest dynamics.

Figure 4.21 illustrates the MSW transform applied to the TMG from Fig. 4.20b. The decreasing sets of markers are obtained by applying h-minima filter, i.e., dynamics of the minima are used. We show two levels in the hierarchy with markers as the regional minima with the n highest dynamics. With $n = 60$, we are able to correctly segment the corpus callosum. With $n = 150$, the corpus callosum is already subdivided into four regions.

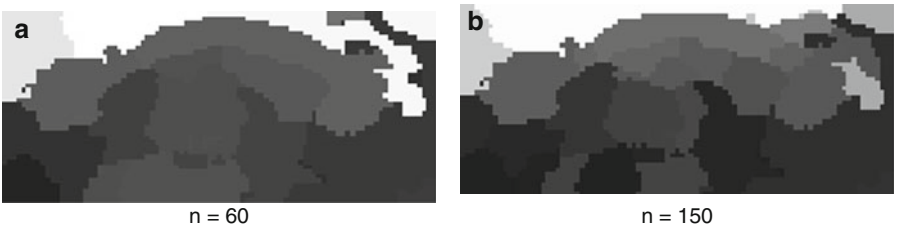

Fig. 4.21. *Multi-scale watershed (MSW).* The MSW transform is computed using the n regional minima with highest dynamics as markers

4.6 Conclusions

Morphological tools are very powerful and useful for biomedical image processing, both for binary and gray-scale images. Unfortunately, they are still not widely known for the majority of the researchers in the field. This chapter illustrated that there are difficult real-world problems that can be solved just using morphological tools. Particularly, there are two important techniques well established such as the watershed-based segmentation and the morphological reconstruction as the primitive operator of a family of component filters.

References

1. Dougherty ER, Lotufo RA. Hands-on Morphological Image Processing. vol. TT59. Bellingham, USA: SPIE Press; 2003.
2. Soille P. Morphological Image Analysis: Principles and Applications. Secaucus, NJ, USA: Springer New York, Inc.; 2003.
3. Lotufo RA, Machado RC, Körbes A, et al. Adessowiki On-line Collaborative Scientific Programming Platform. In: WikiSym '09: Proceedings of the 5th International Symposium on Wikis and Open Collaboration. New York: ACM; 2009. p. 1–6.
4. Lotufo RA, Audigier R, Saúde A, et al. Morphological image processing. In: Microscope Image Processing. Burlington: Academic; 2008. p. 113–158.
5. Serra J. Morphological filtering: an overview. Signal Process. 1994;38(1):3–11.
6. Haralick RM, Sternberg SR, Zhuang X. Image analysis using mathematical morphology. IEEE Trans Pattern Anal Mach Intell. 1987;9(4):532–50.
7. Vincent L. Morphological grayscale reconstruction in image analysis: applications and efficient algorithms. IEEE Trans Image Process. 1993;2(2):176–201.
8. Salembier P, Serra J. Flat zones filtering, connected operators, and filters by reconstruction. IEEE Trans Image Process. 1995;4(8):1153–60.
9. Salembier P, Oliveras A, Garrido L. Anti-extensive connected operators for image and sequence processing. IEEE Trans Image Process. 1998;7(4):555–70.
10. Vincent L. Gray scale area opening and closing, their efficient implementation and applications. In: Serra J, Salembier P, editors. Mathematical Morphology and Its Applications to Signal Processing. Barcelona: UPC Publications; 1993. p. 22–27.

11. Grimaud M. A new measure of contrast: the dynamics. Proc SPIE. 1992; 1769:292–305.
12. Beucher S, Meyer F. The morphological approach to segmentation: the watershed transformation. In: Mathematical Morphology in Image Processing. New York: Marcel Dekker; 1992. p. 433–481.
13. Vincent L, Soille P. Watersheds in digital spaces: an efficient algorithm based on immersion simulations. IEEE Trans Pattern Anal Mach Intell. 1991;13(6):583–98.
14. Lotufo RA, Falcão AX. The ordered queue and the optimality of the watershed approaches. In: Goutsias J, Vincent L, Bloomberg DS, editors. Mathematical Morphology and Its Applications to Image and Signal Processing. vol. 18. Dordrecht: Kluwer; 2000. p. 341–350.
15. Symms M, Jager HR, Schmierer K, et al. A review of structural magnetic resonance neuroimaging. J Neurol Neurosurg Psychiatry. 2004;75(9):1235–44.
16. Dong Q, Welsh RC, Chenevert TL, et al. Clinical applications of diffusion tensor imaging. J Magn Reson Imag. 2004;19(1):6–18.
17. Zhukov L, Museth K, Breen D, et al. Level set modeling and segmentation of DT-MRI brain data. J Electron Imaging. 2003;12:125–133.
18. Wang Z, Vemuri B. DTI segmentation using an information theoretic tensor dissimilarity measure. IEEE Trans Med Imaging. 2005;24(10):1267–77.
19. Jonasson L, Bresson X, Hagmann P, et al. White matter fiber tract segmentation in DT-MRI using geometric flows. Med Image Anal. 2005;9(3):223–36.
20. Weldeselassie Y, Hamarneh G. DT-MRI segmentation using graph cuts. Proc SPIE. 2007;6512:1K-1–9.
21. Lenglet C, Rousson M, Deriche R. A statistical framework for DTI segmentation. Proc IEEE ISBI. 2006;794–97
22. Niogi SN, Mukherjee P, McCandliss BD. Diffusion tensor imaging segmentation of white matter structures using a reproducible objective quantification scheme (ROQS). NeuroImage. 2007;35:166–74.
23. Pierpaoli C, Basser PJ. Toward a quantitative assessment of diffusion anisotropy. Magn Reson Med. 1996;36(6):893–906.
24. Alexander D, Gee J, Bajcsy R. Similarity measures for matching diffusion tensor images. Proc Br Mach Vis Conf. 1999;1:93–102.